

Proceedings of the Second Annual LHCP
ATL-PHYS-PROC-2014-111
September 2, 2014

Reconstruction and identification of hadronic decays of tau leptons in ATLAS

ZINONAS ZINONOS

*On behalf of the ATLAS Experiment,
II. Physikalisches Institut, Georg-August-Universität Göttingen,
Friedrich-Hund-Platz 1, 37077 Göttingen, Germany*

ABSTRACT

Hadronically decaying tau leptons are of prime importance in numerous physics analyses in ATLAS. The spectrum of the possible applications of hadronically decaying tau leptons reaches from Standard Model measurements, including

Higgs searches, to searches for physics beyond the Standard Model.

The basic principles behind the sophisticated tau reconstruction and identification techniques, which are specifically designed to identify hadronically decaying taus and reject various background processes, are delineated here along with current data-driven estimates of their respective performance.

PRESENTED AT

The Second Annual Conference
on Large Hadron Collider Physics
Columbia University, New York, U.S.A
June 2-7, 2014

1 Introduction

Hadronically decaying tau leptons (τ_{had}) play an important role in physics analyses in ATLAS [1]. Their field of application reaches from Standard Model measurements, including Higgs searches [2], to searches for physics beyond the Standard Model [3]. Therefore, the reconstruction and identification algorithms of hadronically-decaying tau leptons have to be continuously adjusted and improved to account for the most up-to-date running conditions and to succeed at overcoming the unprecedented experimental challenges faced by the LHC running at higher than ever energies and luminosities.

For the 2012 data-taking period, the τ_{had} reconstruction and identification schemes have been specifically re-optimized for the high number of simultaneous collisions per proton-proton bunch crossing (pile-up).

2 Reconstruction of Hadronic Tau Decays

Hadronic tau candidates are reconstructed starting from clusters in the electromagnetic and hadronic calorimeters [4]. The τ_{had} reconstruction is seeded by the anti- k_t jet finding algorithm with a distance parameter of $R = 0.4$. A barycenter is formed consisting of the sum of the four-vectors of the constituent topological clusters, assuming zero mass for each of the constituents. Then, the τ_{had} detector axis is calculated by using clusters within $\Delta R = \sqrt{(\Delta\eta)^2 + (\Delta\phi)^2} < 0.2$ around the barycenter. The four-vectors of those clusters are recalculated using the tau vertex coordinate system and the vectors are summed up. Because hadronic tau decays consist of a specific mixture of charged and neutral pions, the energy scale of τ_{had} candidates is adjusted independently of the jet energy scale. The reconstructed energy of τ_{had} candidates is calculated to the final energy scale by a simulation-based calibration procedure using clusters, within $\Delta R < 0.2$ of the seed jet-object barycentre axis. Tracks in a cone of radius $\Delta R < 0.2$ from the cluster barycentre, known as the *core cone*, are associated to the τ_{had} candidate, and the electric charge is determined from the sum of the charges of the tracks. Tracks within the *isolation annulus*, defined by $0.2 < \Delta R < 0.4$ of the τ_{had} axis, are also counted for variable calculations.

3 Identification of Hadronic Tau Decays

3.1 Discrimination against Jets

The rejection of jets is provided in a separate identification step using discriminating variables based on tracks with $p_T > 1$ GeV and calorimeter cells found in the core region and in the isolation annulus around the τ_{had} candidate direction.

On average, jets are wider than hadronic tau decays with a given momentum. Therefore, different variables describing the shower shape in both the calorimeters and the tracking detectors are used to separate τ_{had} from jets, with the most important calorimeter shape variable being the fraction of the total tau energy contained in the centermost cone defined by $\Delta R < 0.1$. Important tracking variables are the average p_T -weighted track distance from the tau axis, and, in multi-prong decays, the distance to the track furthest from the tau axis. Such discriminating variables are combined in a boosted decision tree (BDT), which is trained separately for 1-prong and 3-prong τ_{had} candidates. Three working points – labeled as *loose*, *medium* and *tight* – are defined, corresponding to target identification efficiencies values of 70%, 60% and 40% for 1-prong and 65%, 55% and 35% for multi-prong τ_{had} candidates, respectively.

Figure 1 shows the inverse background efficiency as a function of signal efficiency for the jet BDT discrimination algorithms. Background rejection factors of 10 – 40 for signal efficiencies of 70% are achieved, going up to 500 for 35% signal efficiency [5].

3.2 Discrimination against Electrons

The characteristic signature of 1-prong τ_{had} can be mimicked by electrons. Despite the similarities of the τ_{had} and electron signatures, there are several properties that can be used to discriminate between them. The most useful examples of such properties are the emission of transition radiation of the electron track and the

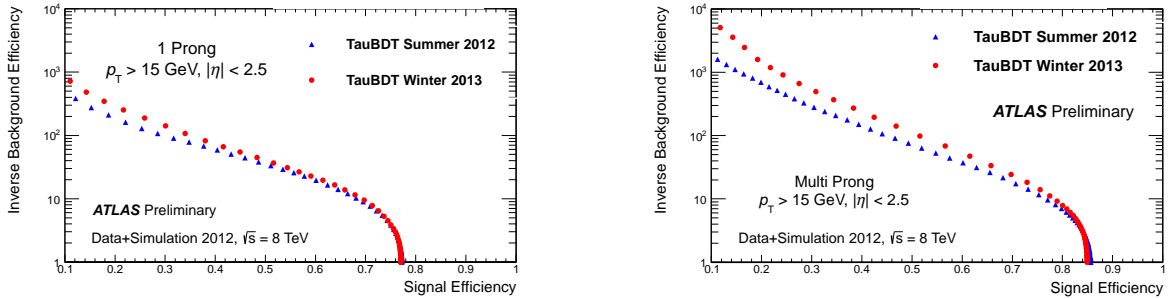


Figure 1: Inverse background efficiency as a function of the signal efficiency with a BDT algorithm for 1-prong $\tau_{\text{had-vis}}$ candidates with a $p_T > 15$ GeV and $|\eta| < 2.5$. The signal efficiencies are obtained using $Z \rightarrow \tau\tau$, $Z' \rightarrow \tau\tau$ and $W \rightarrow \tau\nu$ simulated events. The background efficiencies are derived using 2012 collision data after applying a multi-jet selection and are calculated with respect to all candidates with exactly one reconstructed track. The Winter 2013 BDT uses π^0 -related variables that increase its performance [5].

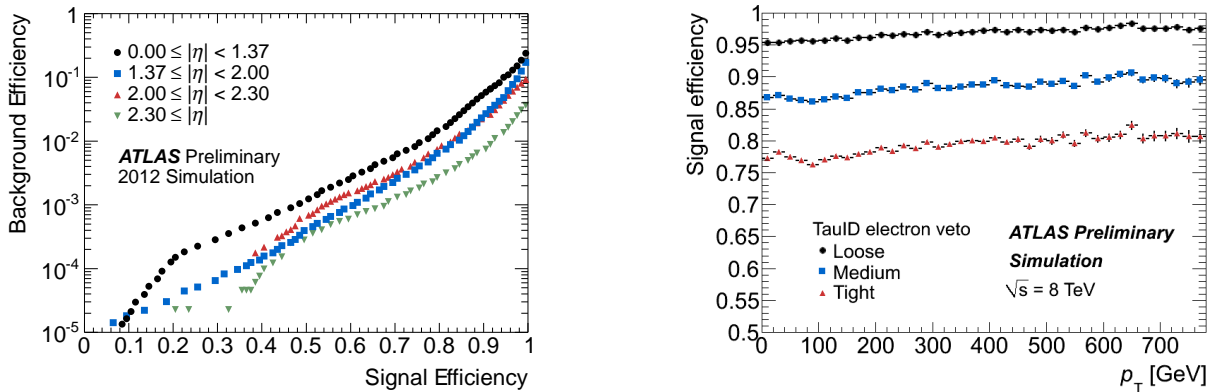


Figure 2: Background efficiency as a function of signal efficiencies of the electron veto for each of the different η regions (left). Signal efficiency of the Winter 2013 electron veto for truth-matched 1-prong tau candidates as a function of reconstructed transverse momentum (right). The efficiencies are obtained using simulated $Z \rightarrow \tau\tau$ events for signal and simulated $Z \rightarrow ee$ events for background [5].

longer and wider showers produced by the hadronic tau decay products in the calorimeter, compared to the one created by an electron. Such properties are used to define τ_{had} identification discriminants specialized in the rejection of electrons mis-identified as hadronically decaying tau leptons. In 2012, the only method for this uses a BDT algorithm. The electron-veto BDT is optimized using simulated $Z \rightarrow \tau\tau$ events for the signal and $Z \rightarrow ee$ events for the background, and was trained for different pseudorapidity (η) regions. The signal versus background efficiencies for the different η regions and the dependence of the efficiency of the electron veto on p_T are shown in Figure 2. The dependence on p_T was such that a sliding cut on the e-veto BDT score was used when implementing the three efficiency working points *loose*, *medium* and *tight*. These working points were chosen to yield signal efficiencies of 95%, 85% and 75%, respectively.

3.3 Discrimination against Muons

As minimum ionizing particles, muons are unlikely to deposit enough energy in the calorimeters to be reconstructed as a τ_{had} candidate. However, when a sufficiently energetic cluster in the calorimeter is associated with a muon, the muon track and the calorimeter cluster together may be mis-identified as a

τ_{had} . Usually, muons which have deposited significant energy in the calorimeter are likely to have done so mostly in the hadronic calorimeter, resulting in τ_{had} candidates with an unusually low electromagnetic energy fraction. Also, for such muons the track momentum may be higher than the calorimeter energy, which is also true of muons that overlap coincidentally with some other calorimeter deposit. Finally, the very low-energy muons must overlap with some other calorimeter energy to pass the τ_{had} reconstruction, and are therefore characterized by a high electromagnetic fraction and low track momentum fraction.

To optimize the muon veto, simulated muons from $Z \rightarrow \mu\mu$ events and hadronic tau decays from $Z \rightarrow \tau\tau$ events were used. The resulting efficiency is better than 96% for true τ_{had} with a reduction of muon fakes around 40% [4].

4 Tau Identification Efficiency Measurement

The identification (ID) efficiency of τ_{had} candidates is studied in data using a ‘tag-and-probe’ approach. From these studies, a set of scale factors, defined as $\epsilon_{\text{data}}/\epsilon_{\text{simulation}}$, is derived to correct the simulated data samples used in physics analyses. These measurements are performed independently using $Z \rightarrow \tau\tau$, $W \rightarrow \tau\nu$ and $t\bar{t} \rightarrow \tau + \text{jets}$ events. Scale factors for the τ_{had} mis-identification probability for electrons are also measured, comparing $Z \rightarrow ee$ events in data and simulations.

The tag-and-probe approach chosen consists of selecting events with real tau leptons in their final state, and extracting a measure of the identification efficiencies directly from the number of reconstructed τ_{had} before and after identification algorithms are applied. To estimate the number of background events, a variable with good separation potential is chosen. A fit is then performed using the expected distributions in this variable (templates) for both signal and backgrounds. The real number of hadronic tau decays in data is then obtained from the fitted signal template. To measure the tau ID efficiency for data, ϵ_{data} , the number of real τ_{had} after tau ID is divided by the number of real τ_{had} before tau ID. The uncertainties on the efficiency measurement are estimated by recalculating the efficiency using systematically altered templates. For the efficiency in simulated samples, $\epsilon_{\text{simulation}}$, the number of tau leptons before and after tau ID is taken directly from truth-matched τ_{had} candidates. Scale factors are therefore calculated to account for the differences between data and simulation due to the modeling of the input variables for the identification algorithms.

The $Z \rightarrow \tau_{\text{lep}}\tau_{\text{had}}$ channel is chosen as the main measurement, as it offers the highest precision due to the low associated backgrounds.

To determine the number of signal and background events in the chosen topologies, a fit to data is used. The signal and the background are modeled with templates, obtained from either simulations or data-driven techniques. The variable chosen for the fit is the extended track multiplicity (performing a p_T -correlated track counting in the $0.2 < \Delta R < 0.6$ annulus around the core cone) associated to the τ_{had} candidate as it provides good separation between the signal and the backgrounds.

The extended track multiplicity distribution after the tag-and-probe selection has been applied, and before and after tau ID criteria have been applied, can be found in Figure 3. In these figures, the multi-jet background is not included as it is later determined using data-driven techniques; this background accounts for most of the difference between the data and simulation.

5 Conclusions

The reconstruction and identification algorithms for hadronically decaying tau leptons for the 2012 data period have been outlined here. A BDT identification algorithm was trained on simulated event samples and data and provides high background rejection and signal efficiency for three pre-determined working points. This discrimination algorithm provides rejection factors against multi-jet backgrounds of the order of 60 to 500 for a signal efficiency of 35%. Dedicated prescriptions are also provided for rejecting electrons or muons being mis-identified as τ_{had} candidates. The electron-veto uses a multi-variate discriminant and was optimized using simulated events, providing three fixed efficiency working points. Rejection factors above 100 against background electrons are attained with the tight working point. The performance of the various

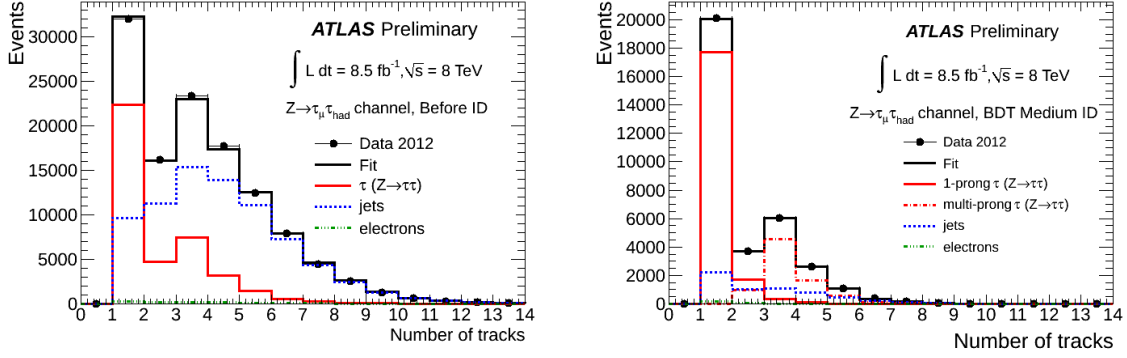


Figure 3: Distribution of the number of tracks associated with hadronically-decaying tau candidates from the $Z \rightarrow \tau\tau$ tag & probe selection in 2012 data, before tau ID (left) and after BDT medium tau ID (right) for the measurement of the 1-prong and multi-prong identification efficiencies. All ID methods and working points are included in the same fit. The tau signal template and the electron template are taken from simulations. The jet template is obtained from data in a control region. The distribution shown is the sum of core and p_T -correlated tracks [5].

identification algorithms was tested in data-driven studies. Measurements of the tau ID algorithm efficiencies were performed using the $Z \rightarrow \tau_{lep}\tau_{had}$, $W \rightarrow \tau_{had}\nu_\tau$, and $t\bar{t} \rightarrow \tau_{had} + \text{jets}$ channels with the goal of providing data for simulation scale factors.

In general, good agreement was found between the performance of the identification algorithms in both simulated events and in data. Scale factors and associated uncertainties, to be used in correcting simulated samples, are provided for the ID algorithms and the electron veto.

References

- [1] ATLAS Collaboration, “The ATLAS Experiment at the CERN Large Hadron Collider,” JINST **3**, S08003 (2008), <https://cds.cern.ch/record/1129811>
- [2] ATLAS Collaboration, “Evidence for Higgs Boson Decays to the $\tau^+\tau^-$ Final State with the ATLAS Detector,” <http://cds.cern.ch/record/1632191>, ATLAS-CONF-2013-108, November 2013, CERN
- [3] ATLAS Collaboration, “Search for charged Higgs bosons in the τ +jets finalstate with pp collision data recorded at $\sqrt{s} = 8$ TeV with the ATLAS experiment,” <http://cds.cern.ch/record/1595533>, ATLAS-CONF-2013-090, August 2013, CERN
- [4] ATLAS Collaboration, “Identification of the Hadronic Decays of Tau Leptons in 2012 Data with the ATLAS Detector,” <http://cds.cern.ch/record/1562839>, ATLAS-CONF-2013-064, July 2013, CERN
- [5] ATLAS Collaboration, <https://twiki.cern.ch/twiki/bin/view/AtlasPublic/TauPublicCollisionPlots>